Mode Conversion Caused by Bending in Photonic Subwavelength Waveguides

Y. J. Rodriguez-Viveros [1], D. Moctezuma-Enriquez [2], P. Castro-Garay [1], B. Manzanares-Martinez [1], C. I. Ham-Rodriguez [3], E. Urrutia-Banuelos [3], and J. Manzanares-Martinez [3]

[1] Departamento de Fisica
Universidad de Sonora, Blvd. Luis Encinas y Rosales, Hermosillo, Sonora 83000, Mexico
yohan.jasdid@gmail.com, paola@cifus.uson.mx, betsabe.manzanares@correo.fisica.uson.mx

[2] Instituto Tecnologico de Hermosillo
Av. Tecnológico s/n, Sonora 83170, Mexico
bersek_no1@hotmail.com

[3] Departamento de Investigacion en Fisica
Universidad de Sonora, Blvd. Luis Encinas y Rosales, Hermosillo, Sonora 83000, Mexico
cavanharz@hotmail.com, eurrutia@cifus.uson.mx, jmanza@cifus.uson.mx

Abstract ─ We study the propagation of light in a subwavelength planar waveguide with an angular bend. We observe the mode conversion of a guided wave with a symmetric beam profile impinging into the bending of a waveguide. The guided wave outgoing from the bend is a mixed set of symmetric and asymmetric modes. The amount of mode conversion through the bend is quantified by calculating the Fourier transform of the electric field profile. It is found that the conversion rate is a function of the bending angle.

Index Terms ─ Bending, mode conversion, subwavelength, waveguide.

I. INTRODUCTION

Optical fibers (OF) are dielectric waveguides in the form of cylinders with a diameter (d) larger than the visible range wavelengths (λ=390 nm to λ=700 nm) [1]. OF are flexible waveguides, however, the angle of bending (θ) is limited by a critical angle (θ_c) defined by the principle of total internal reflection (TIR) [1]. They are widely used in optical networks, sensors and other devices [2, 3]. Nowadays to control the flow of data on the Telecom Industry, optical and electronic devices coexist. On the one hand, for long distances photons are transported via optical fibers, which support high bandwidths with low losses. On the other hand, in the electronic circuitry the essential functions of switching and routing are made by manipulating the flow of electrons. The bottleneck for data transfer in this hybrid technology is the operation frequency of the electronic processor which currently is of only a few GHz [4]. To increase the speed of data transfer in optical networks, it has been proposed the development of photonic integrated circuits (PIC) [5, 6]. A PIC does analogous main functions to those of electronic integrated circuits (EIC). The difference is that PIC provides a direct manipulation of the photons traveling in optical waveguides. It is expected that the processing of light in PIC overcome the physical limitations of speed and power dissipation faced by EIC [7].

A progressive development of PIC has been made in the last two decades, which can be classified on three main approaches. A first approach is based on the use of photonic crystals (PC) as a framework for the design of photonic devices to control the flow of light [6]. PC are periodic dielectric structures composed by at least two materials in the unit cell of period (a) which is on the order of the visible wavelength, $a \sim \lambda$ [8]. The fundamental characteristic of PC is the existence of photonic band gaps (PBG) where photons cannot propagate through the periodic lattice. Photonic devices on the order of visible wavelengths can be engineered in PC introducing localized states in the PBG by removing unit cells in the otherwise perfect crystal [9]. A second strategy to design PIC is based on the use of plasmons [10]. Plasmon-based approaches require a precise manipulation of the electromagnetic fields, which are exponentially decaying from the surfaces [11]. It has been suggested the possibility of creating surface-plasmon circuitry with photonic components smaller than the diffraction limit of light [12]. Plasmons however, have substantial optical losses which can severely limit their applicability [13]. To overcome these losses, it has recently been proposed

Submitted On: January 6, 2015
Accepted On: November 7, 2015

the use of gain-loss structures, which introduce unusual possibilities for the propagation of plasmons [14]. A third approach to fabricate PIC is based on the use of nanowires [15-17]. OF and nanowires are both cylindrical waveguides of a diameter d. However, OF have a diameter much bigger than the visible wavelength ($d > \lambda$) which allow a multimodal propagation. In contrast, the nanowire diameter is smaller than the visible wavelength ($d < \lambda$) and as a consequence, only the propagation of a few modes is allowed. This characteristic is desirable for the fabrication of PIC because it is possible to have a more precise control and manipulation of light.

In the last decade, an intensive effort has been made to reduce the width of waveguides [17]. The fabrication of optical waveguides with diameters smaller than the wavelength is a difficult task. For many years it was not possible to attain nanowires with a good quality fabrication because of inherent disorder in the fabrication process such as the existence of surface roughness and diameter variations [16]. In 2003, Tong et al. reported an experimental technique that allowed fabricating wires with diameters as small as 50 nm with an excellent quality [17]. These subwavelength nanowires allowed a higher confinement of photons in small volume regions opening new possibilities for both, the study of fundamental properties and their integration into functional devices [17, 18]. The use of subwavelength waveguides has spun the development of at least five fundamental building blocks for photonic circuitry: i) light sources (lasers) [19], ii) passive components (interconnects) [20], iii) active components (transistors) [21], iv) nonreciprocal optical isolators (diodes) [22], and v) light detectors [23].

Recently Voss et al. investigated the waveguiding at the intersection of two nanowires, which were dissimilar in materials and diameters [24]. One of the main results was the experimental evidence of the excitation of high-order modes, as a result of slight changes in the alignment between subwavelength nanowires. Another important result was the in-situ observation of the generation of high-order modes at imperfections of a nanowire. These results experimentally confirmed the phenomena of mode conversion in subwavelength nanowires

Mode conversion has been recently studied for two other cases of waveguide bends. In the first case, Xing et al. analyzed the propagation of spin-waves passing through a bended magnetic waveguide at the submicron scale using micro-magnetic simulations [25]. In the second case, Zhang et al. studied theoretically and experimentally the TE_{10}-TE_{20} mode conversion of a rectangular waveguide at the microwave regime [26]. In these cases the possibility of separating the fields after the mode conversion into different waveguide branches was reported. In both cases, it has been found that it's possible to have a phase shift between branches as a result of the path difference. In particular, in Ref. [25] it was demonstrated the possibility of creating a kind of Mach-Zehnder interferometer where logic-NOT and logic-AND gates can be tuned in frequency. This result opens the possibility of integrating the mode conversion into interferometric devices.

II. THEORY

The propagation of the electromagnetic fields in a planar waveguide is analyzed by using the curl Maxwell's equations:

$$\nabla \times \mathbf{H}(\mathbf{x}, t) = \frac{\partial}{\partial t}\mathbf{D}(\mathbf{x}, t), \quad (1)$$

$$\nabla \times \mathbf{B}(\mathbf{x}, t) = -\frac{\partial}{\partial t}\mathbf{E}(\mathbf{x}, t). \quad (2)$$

For the Eq. (1) we have considered the case where the density of current is zero, $\mathbf{J}(\mathbf{x}, t) = 0$. Maxwell equations are complemented by the constitutive relations that introduces the material electromagnetic properties of the physical problem. The electric permittivity (ε) provides a description of the macroscopic interaction between the electric field and the dielectric material, whereas the magnetic permeability (μ) describes the interaction of the material with the magnetic field. For the case of a dielectric material (without dispersion), these relations can be written in the form:

$$\mathbf{D}(\mathbf{x}, t) = \varepsilon(\mathbf{x})\mathbf{E}(\mathbf{x}, t), \quad (3)$$

$$\mathbf{B}(\mathbf{x}, t) = \mu(\mathbf{x})\mathbf{H}(\mathbf{x}, t). \quad (4)$$

In Fig. 1 we present the basic geometry of a planar waveguide composed by a slab of high refractive index (n_h) and width d, which is sandwiched between two semi-infinite media of low refractive index (n_l). In this work, we analyze the case of the transversal electric (TE) polarization, where the electric field is parallel to the z-axis, $\boldsymbol{E}(\boldsymbol{x}, t) = \hat{k}E_z(x, y, t)$. The electromagnetic waves inside and outside the slab are propagating and evanescent, respectively.

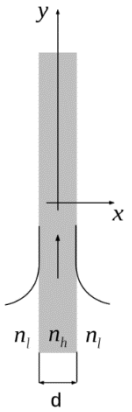

Fig. 1. Planar waveguide of width d and refractive index n_h between two semi-infinite media of refractive index n_l.

The dispersion relation is obtained by solving two well-known transcendental equations [27]. On the one hand, the condition for the modes of even parity with

respect to the *x*-axis is given by the equation:

$$\tan(\pi Q_{x,h}) = Q_{x,l}/Q_{x,h}. \quad (5)$$

On the other hand, the condition for the modes with odd parity is:

$$\cot(\pi Q_{x,h}) = -Q_{x,l}/Q_{x,h}. \quad (6)$$

The reduced wave vectors in the *x*-axis for the high and low refractive index media are:

$$Q_{x,h} = \sqrt{n_h^2\Omega^2 - Q_y^2}, \quad (7)$$

$$Q_{x,l} = \sqrt{Q_y^2 - n_l^2\Omega^2}. \quad (8)$$

The reduced frequency is:

$$\Omega = \omega d/2\pi c. \quad (9)$$

And the reduced wavevector in the *y*-axis is:

$$Q_y = k_y d/2\pi. \quad (10)$$

Figure 2 presents the dispersion relation for the planar waveguide. The high and low refractive indices are n_h=2 and n_l=1, which correspond to the refractive index of ZnO nanowires in air, according to Refs. [18, 24]. Q_y and Ω are the abscissa and ordinate axis, respectively. The light gray zone (Ω<0.3) is the monomodal frequency regime where only one eigenmode is allowed. Conversely, the dark-gray zone (Ω>0.3) is the multimodal frequency regime where two or more eigenmodes are allowed. The TE_0 and TE_1 modes correspond to the first even and odd solutions, respectively. In the monomodal regime, we identify the α eigenmode at (0.32,0.2) which belongs to the TE_0 mode. At the multimodal region we identify the β eigenmode at (0.49,0.4) and the γ eigemode at (0.72,0.4), which correspond to the TE_1 and TE_0 modes, respectively. The arrow line from γ to β illustrates the conversion of modes that we analyze below.

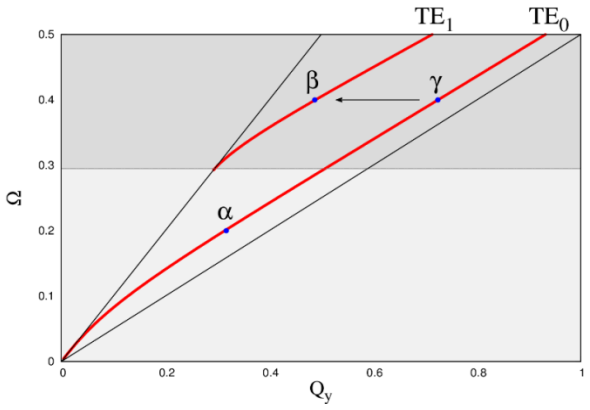

Fig. 2. Dispersion relation for a planar waveguide. The light and dark gray regions are the monomodal and multimodal regimes. The α and γ points belong to the TE_0 mode, while the β point is part of the TE_1 mode.

In Fig. 3 we present the electric field profile for the α, β and γ eigenmodes. We observe that the TE_0 modes corresponding to the α and γ eigenmodes in Fig. 3 (a) and Fig. 3 (c) have an even symmetry. Correspondingly, the TE_1 mode corresponding to the β eigenmode in Fig. 3 (b) has an odd symmetry.

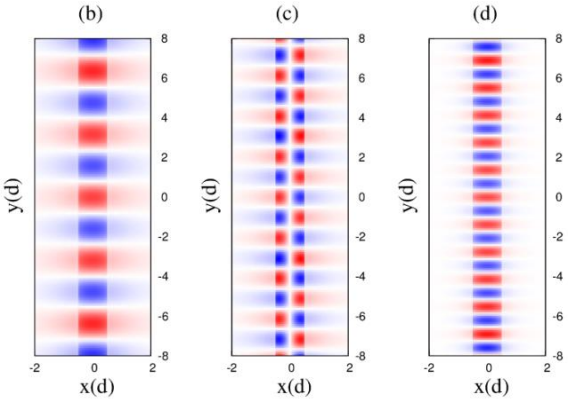

Fig. 3. The electric field profile for the α, β and γ eigenmodes are presented in (a), (b) and (c).

III. NUMERICAL METHOD

We simulate the propagation of the electromagnetic field in the planar waveguide using the finite difference time domain (FDTD) method [28]. The FDTD method is a computational technique used for modeling the temporal evolution of the Maxwell equations. This numerical method is based on the formulation of the differential equations in an associate system of equations in finite differences. The time-dependent Maxwell's equations are discretized using a central-difference approximation to the space and time partial derivatives. The resulting finite-difference system of equations is reformulated in terms of a computational algorithm that can be solved in the time-domain using a recursive process.

In this work, we have simulated the propagation of the electromagnetic field using Phoxonics, the software that we have designed to implement the FDTD technique [29]. Phoxonics is a sophisticated and flexible computational program that allows studying different geometric configurations. In particular, we have analyzed the mode conversion caused by the bending of a planar waveguide.

Considering a polarization of the electric field $\boldsymbol{E}(\boldsymbol{x},t) = \hat{k}E_z(x,y,t)$, the Maxwell's equations (1) and (2) can be written as three scalar equations in the form:

$$\frac{\partial}{\partial t}D_z(x,y,t) = \frac{\partial}{\partial x}H_y(x,y,t) - \frac{\partial}{\partial y}H_x(x,y,t), \quad (11)$$

$$\frac{\partial}{\partial y}E_z(x,y,t) = -\frac{\partial}{\partial t}B_x(x,y,t), \quad (12)$$

$$\frac{\partial}{\partial x}E_z(x,y,t) = \frac{\partial}{\partial t}B_y(x,y,t). \quad (13)$$

The set of scalar Equations (11)-(13) can be reformulated in terms of finite differences. The finite-difference version of the Equation (11) at the point $(x,y,t) = (i\Delta x, j\Delta y, n\Delta t)$ is:

$$\frac{D_z\left(i,j,n+\frac{1}{2}\right)-D_z\left(i,j,n-\frac{1}{2}\right)}{\Delta t} = \frac{H_y\left(i+\frac{1}{2},j,n\right)-H_y\left(i-\frac{1}{2},j,n\right)}{\Delta x} - \frac{H_x\left(i,j+\frac{1}{2},n\right)-H_x\left(i,j-\frac{1}{2},n\right)}{\Delta y}. \quad (14)$$

The Eq. (12) is written in finite differences for the point $(x,y,t)=\left[i\Delta x,\left(j+\frac{1}{2}\right)\Delta y,\left(n+\frac{1}{2}\right)\Delta t\right]$ as:

$$\frac{B_x\left(i,j+\frac{1}{2},n+1\right)-B_x\left(i,j+\frac{1}{2},n\right)}{\Delta t} = \frac{E_z\left(i,j+1,n+\frac{1}{2}\right)-E_z\left(i,j,n+\frac{1}{2}\right)}{\Delta y}. \quad (15)$$

Finally, the Eq. (13) in finite differences for the point $(x,y,t)=\left[\left(i+\frac{1}{2}\right)\Delta x,j\Delta y,\left(n+\frac{1}{2}\right)\Delta t\right]$ is:

$$\frac{B_y\left(i+\frac{1}{2},j,n+1\right)-B_y\left(i+\frac{1}{2},j,n\right)}{\Delta t} = \frac{E_z(i+1,j,n+1/2)-E_z(i,j,n+1/2)}{\Delta x}. \quad (16)$$

To establish the set of finite difference Equations (14)-(16) in terms of a numerical algorithm, we write these equations in a leapfrog manner that can be solved recursively by using a computational program. To validate the computational implementation of the FDTD method using Phoxonics, we consider a planar waveguide with one or two monochromatic sources embedded inside. These sources are placed at the bottom of our simulation grid to allow seeing the excitation of the eigenmodes. For the case of the α and γ even-modes, they can be excited with a single monochromatic source that is defined by:

$$E_z(x,y,t)=A_1\delta(x-w_{1x})\delta(y-w_{1y})\sin(\omega t). \quad (17)$$

To excite the β mode, it is necessary to consider two monochromatic sources defined by:

$$E_z(x,y,t)=\left[A_1\delta(x-w_{1x})\delta\left(y-w_{1y}\right)+A_2\delta(x-w_{2x})\delta\left(y-w_{2y}\right)\right]\sin(\omega t). \quad (18)$$

The points (w_{1x},w_{1y}) and (w_{2x},w_{2y}) define the position of the monochromatic sources on the x and y axes. A_1 and A_2 are the amplitudes of the sources. The frequency of the monochromatic sources is ω.

The excitation of the α and γ eigenmodes using FDTD is obtained by considering a single monochromatic source, as it is defined in Eq. (17). The position of the monochromatic source is $\left(w_{1x},w_{1y}\right)=(0,-8d)$. In Figs. 4 (a) and 4 (c), the spatial distribution of the TE_0 mode is illustrated when the sources are emitting at the reduced frequencies $\Omega=0.2$ and $\Omega=0.4$, respectively. To obtain the excitation of the β eigenmode we need to use two monochromatic sources as it is defined in Eq. (18). The amplitude of the sources are $A_1=1$ and $A_2=-1$. The position of the sources are $\left(w_{1x},w_{1y}\right)=(-0.4d,-8d)$ and $\left(w_{2x},w_{2y}\right)=(+0.4d,-8d)$, respectively. In Fig. 4 (b) we present the distribution of the TE_1 mode for the case where both monochromatic sources are emitting at a reduced frequency of $\Omega=0.4$.

To validate the excitation of the α, β and γ modes in the planar waveguide using the FDTD technique, we calculate the Fourier transform (FT) of the electric field by using the formula:

$$E_z(Q_y)\cong\frac{1}{\sqrt{2\pi}}\int_0^{L_y}E_z(y)\,e^{i2\pi Q_y y/d}dy. \quad (19)$$

The limits of integration have been switched to consider the finite interval [0:L_y].

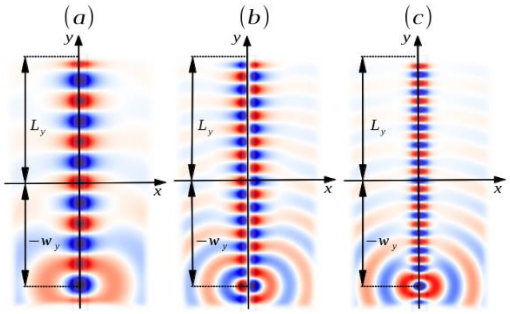

Fig. 4. Simulation of the electric field propagation using FDTD. The excitation of the α, β and γ eigenmodes are presented in (a), (b) and (c), respectively.

In Fig. 5 we present the FT for the electric field on the surface of the planar waveguide. The FT of the electric field distributions in Fig. 3 (a), Fig. 3 (b) and Fig. 3 (c) is presented in Fig. 5 with dotted, dashed and solid lines, respectively. From left to right, the FT peaks around the reduced wavevectors Q_y=0.32, Q_y=0.49 and Q_y=0.72 prove the existence of the α, β and γ eigenmodes, respectively.

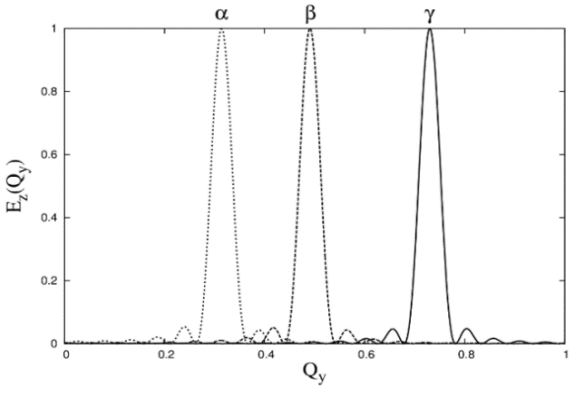

Fig. 5. Fourier transform of the electric field at the surface of the planar waveguide. From left to right, the dotted, dashed and solid lines are the α, β and γ modes.

IV. MODE CONVERSION

In this section, we analyze the mode conversion caused by a bending in a planar waveguide. We consider the case where the TE_0 impinges into the bend. In Fig. 6 is shown a planar waveguide with a bend angle θ at the vicinity of the coordinate system origin.

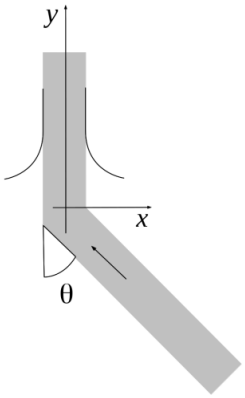

Fig. 6. A planar waveguide with a bend angle θ. The bend is placed at the vicinity of the coordinate system origin.

In Fig. 7 we simulate the propagation of light in the monomodal regime. An even beam profile corresponding to the TE_0 mode with a reduced frequency Ω=0.2 is impinging into the waveguide bend. The cases of waveguides bended with angles of θ=15°, θ=30°, and θ=90°, are presented in (a), (b) and (c), respectively. There are three important observations. The first one is that the incident guided wave passes through the bending without distortion in his symmetry. The second is that the propagation of guided light is not limited by any critical bending angle, as it exists in conventional OF as consequence of the TIR. And the third is that the bending emission increases with the bend angle.

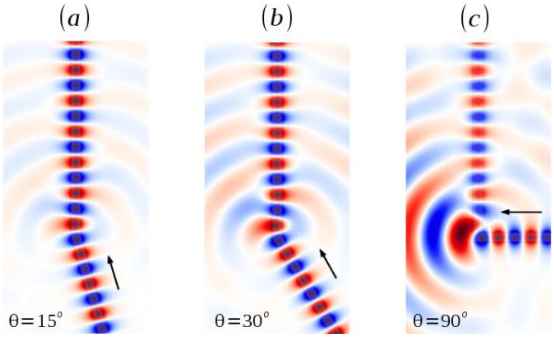

Fig. 7. Propagation at the monomodal regime (Ω=0.2) of the TE_0 mode through a waveguide with an angular bend θ. The cases θ=15°, 30° and 90° are presented in (a), (b) and (c).

In Fig. 8 we simulate the propagation at the multimodal regime. Here, the TE_0 mode is impinging into the bend with a reduced frequency Ω=0.4. For the case of θ=15° illustrated in Fig. 8 (a), we observe that a slight deformation on the geometry of the electric field profile exists. In Fig. 8 (b) is shown the case for θ=30°, for which we observe that after the bend there is a mixed profile of the TE_0 and TE_1 modes where it is not possible to identify a predominant even or odd symmetry. Finally, in Fig. 8 (c) we present the case of θ=90°. It is evident that the incoming mode TE_0 is converted after the bend into the TE_1 mode.

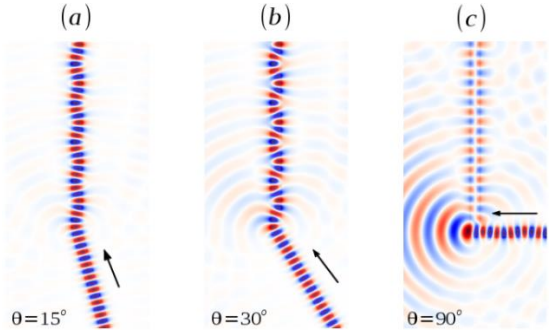

Fig. 8. Propagation at the multimodal regime (Ω=0.4) of the TE_0 mode through a waveguide with an angular bend θ. The cases θ=15°, 30° and 90° are presented in (a), (b) and (c).

The mode conversion can be quantified by using the FT of the electric field as it is defined in in Eq. (19). The FT is calculated for the electric field after the bend on the surface of the planar waveguide. We consider the case presented in Fig. 8, where a guided wave of TE_0 mode is impinging into the bending with a reduced frequency of Ω=0.4.

In Fig. 9 we present the FT for the cases corresponding to an angle of bend θ=0°, 15°, 30° and 60° using black, blue, green and red lines, respectively. We observe that as the angle of bend increases, the amplitude corresponding to the γ mode diminishes. Conversely, as the angle of bend increases the amplitude of the β mode increases. Thus after the bend, the amplitude of the TE_0 mode decreases and the TE_1 mode increases, in both cases as function of the bend angle.

In Fig. 10 we present the variation of the TE_0 and TE_1 modes as a function of the angle θ using a solid and dashed lines, respectively. It is observed that the amount of the TE_0 mode decreases monotonously as a function of the angle of bend. It is found that the TE_0 mode disappear after the bend when is reached θ=80°. In contrast, the amount of the TE_1 mode increases as a function of the angle of bend in the range from 0° to 60°. At 60°, the amount of TE_1 mode starts to decrease. We

observe that for the bend angle θ=90° a complete mode conversion occurs.

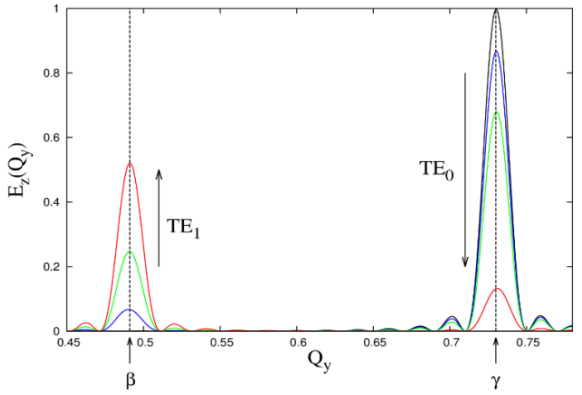

Fig. 9. Fourier transform of the electric field after the bending. The cases θ=0°, 15°, 30° and 60° are presented with black, blue, green and red lines, respectively.

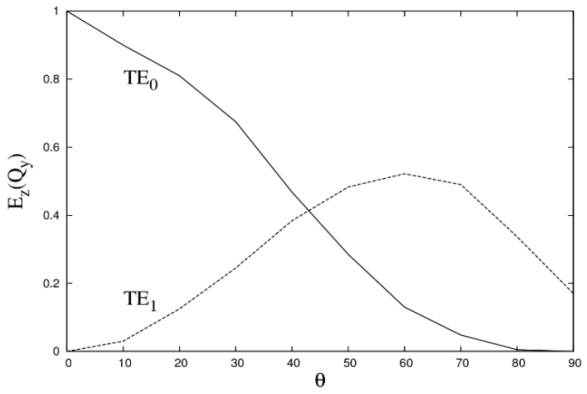

Fig. 10. Fourier transform of the electric field profile as a function of θ. The amplitude of the TE_0 and TE_1 modes are presented with solid and dashed lines, respectively.

V. CONCLUSION

In conclusion, these results demonstrate that subwavelength bend waveguides not just passively transmit light from one point to another. At the multimodal regime, the bend of a subwavelength waveguide acts as a mode converter exciting high-order modes. Therefore, the waveguide bend needs to be intrinsically considered as an active device because it causes a spatial redistribution of the fields. This phenomenon provides an opportunity to create logic devices based in the mode conversion.

We have found a strategy to identify the mode conversion by calculating the FT of the distribution of electric field after the bending. Finally, this study based on the analysis of a two-dimensional geometry is a first step to better understand and utilize the mode conversion in three-dimensional nanowires, which is an essential step for the design of PIC based in subwavelength waveguides.

ACKNOWLEDGMENT

We thank Professor Julio Saucedo for carefully reading the manuscript. This work has been supported by the CONACYT-104151 project. We thank PROMEP-Mexico by special support Grant FOFM-2008.

REFERENCES

[1] J. D. Jackson, *Classical Electrodynamics*, Wiley, New York, 1998.

[2] J. P. Goure and I. Verrier, *Optical Fibre Devices*, CRC Press, New York, 2001.

[3] Optics Communications. *Special Issue: Optical Micro/Nanofibers: Challenges and Opportunities*, vol. 285, no. 4641, 2012.

[4] J. D. Meindl, "Beyond Moore's law: the interconnect era," *Computing in Science Engineering*, vol. 5, pp. 20-24, 2003.

[5] L. Coldren and S. Corzine, *Diode Lasers and Photonic Integrated Circuits*, Wiley, New York, 2012.

[6] J. D. Joannopoulos, P. R. Villeneuve, and S. Fan, "Photonic crystals: putting a new twist on light," *Nature*, vol. 386, pp. 143-149, 1997.

[7] X. Guo, Y. Ying, and L. Tong, "Photonic nanowires: from subwavelength waveguides to optical sensors," *Accounts of Chemical Research*, vol. 47, pp. 656-666, 2014.

[8] E. Yablonovitch, "Inhibited spontaneous emission in solid-state physics and electronics," *Phys. Rev. Lett.*, vol. 58, pp. 2059-2062, 1987.

[9] J. Joannopoulos, R. Meade, and J. Winn, *Photonic Crystals*, Princeton Press, Princeton, 1995.

[10] S. Hayashi and T. Okamoto, "Plasmonics: visit the past to know the future," *Journal of Physics D: Applied Physics*, vol. 45, 433001, 2012.

[11] E. Ozbay, "Plasmonics: Merging Photonics and Electronics at Nanoscale Dimensions", Science, vol. 311, pp. 189-193, 2006.

[12] T. W. Ebbesen, C. Genet, and S. I. Bozhevolnyi, "Surface plasmon circuitry," *Physics Today*, vol. 61, pp. 44-50, 2008.

[13] M. Kuttge, E. J. R. Vesseur, J. Verhoeven, H. J. Lezec, H. A. Atwater, and A. Polman, "Loss mechanisms of surface plasmon polaritons on gold probed by cathodoluminescence," *Applied Physics Letters*, vol. 93, 113110, 2008.

[14] J. Manzanares-Martinez, C. I. Ham-Rodriguez, D. Moctezuma-Enriquez, and B. Manzanares-Martinez, "Omnidirectional mirror based on Bragg stacks with a periodic gain-loss modulation," *AIP Advances*, vol. 4, 017136, 2014.

[15] P. J. Pauzauskie and P. Yang, "Nanowire photonics," *Materials Today*, vol. 9, pp. 36-45, 2006.

[16] F. Ladouceur, "Roughness, inhomogeneity, and integrated optics," *Journal of Lightwave Technology*,

vol. 15, pp. 1020-1025, 1997.

[17] L. Tong, R. Gattass, J. Ashcom, S. He, J. Lou, M. Shen, I. Maxwell, and E. Mazur, "Subwavelength-diameter silica wires for low-loss optical wave guiding," *Nature*, vol. 426, pp. 816-819, 2003.

[18] T. Voss, G. T. Svacha, E. Mazur, S. Mller, C. Ronning, D. Konjhodzic, and F. Marlow, "High-order waveguide modes in ZnO nanowires," *Nano-Letters*, vol. 7, pp. 3675-3680, 2007.

[19] D. O'Carroll, I. Lieberwirth, and G. Redmond, "Microcavity effects and optically pumped lasing in single conjugated polymer nanowires," *Nature Nanotechnology*, vol. 2, pp. 180-184, 2007.

[20] M. Law, D. Sirbuly, J. Johnson, J. Goldberger, R. Saykally, and P. Yang, "Nanoribbon waveguide for subwavelength photonics integration," *Science*, vol. 305, pp. 1269-1273, 2004.

[21] D. Powell, "Light flips transistor switch," *Nature*, vol. 498, pp. 149-149, 2013.

[22] D. Jalas, A. Petrov, M. Eich, W. Freude, S. Fan, Z. Yu, R. Baets, M. Popovic, A. Melloni, J. D. Joannopoulos, M. Vanwolleghem, C. R. Doerr, and H. Renner, "What is -and what is not- an optical isolator," *Nature Photonics*, vol. 7, pp. 579-582, 2013.

[23] J. Wang, M. Gudiksen, X. Duan, Y. Cui, and C. Lieber, "Highly polarized photoluminescence and photodetection," *Science*, vol. 293, pp. 1455-1457, 2001.

[24] T. Voss, "Waveguiding and optical coupling in ZnO nanowires and tapered silica fibers," *Advances in Solid State Physics*, vol. 48, pp. 57-64, 2009.

[25] X. Xing, Y. Yo, S. Li, and X. Huang, "How do spin waves pass through a bend?," *Scientific Reports*, vol. 3, 2958, 2013.

[26] Q. Zhang, C.-W. Yuan, and L. Liu, "Theoretical design and analysis for the TE_{20}-TE_{10} rectangular waveguide mode converters," *IEEE Transactions on Microwave Theory and Techniques*, vol. 60, pp. 1018-1025, 2012.

[27] P. Yeh, *Optical Waves in Layered Media*, Wiley, New York, 1998.

[28] K. S. Yee, "Numerical solution of initial boundary value problems involving Maxwell's equations in isotropic media," *IEEE Trans. Antennas Propagat*., vol. 14, pp. 302-307, 1966.

[29] http://phoxonics.com/software.